Supporting Information

Robust Conductive Gel-Infused Sponge-based Triboelectric Nanogenerator for Reliable Long-Term Self-Powered Electronics and Wireless Monitoring

Sakshi Dhiman [a, b], Bablesh Gupta [a, b], Aayush Dabrey [c], Ranbir Singh[a, b] *

[a] *School of Mechanical and Materials Engineering, Indian Institute of Technology Mandi, Kamand, Mandi, Himachal Pradesh, 175005, India*

[b] *Advanced Energy Conversion Laboratory (AECL), Indian Institute of Technology Mandi, Kamand, Himachal Pradesh, 175005, India*

[c] *Engineering Physics, National Institute of Technology (NIT), Hamirpur, 177005, India*

Corresponding Email ID: *ranbir@iitmandi.ac.in*

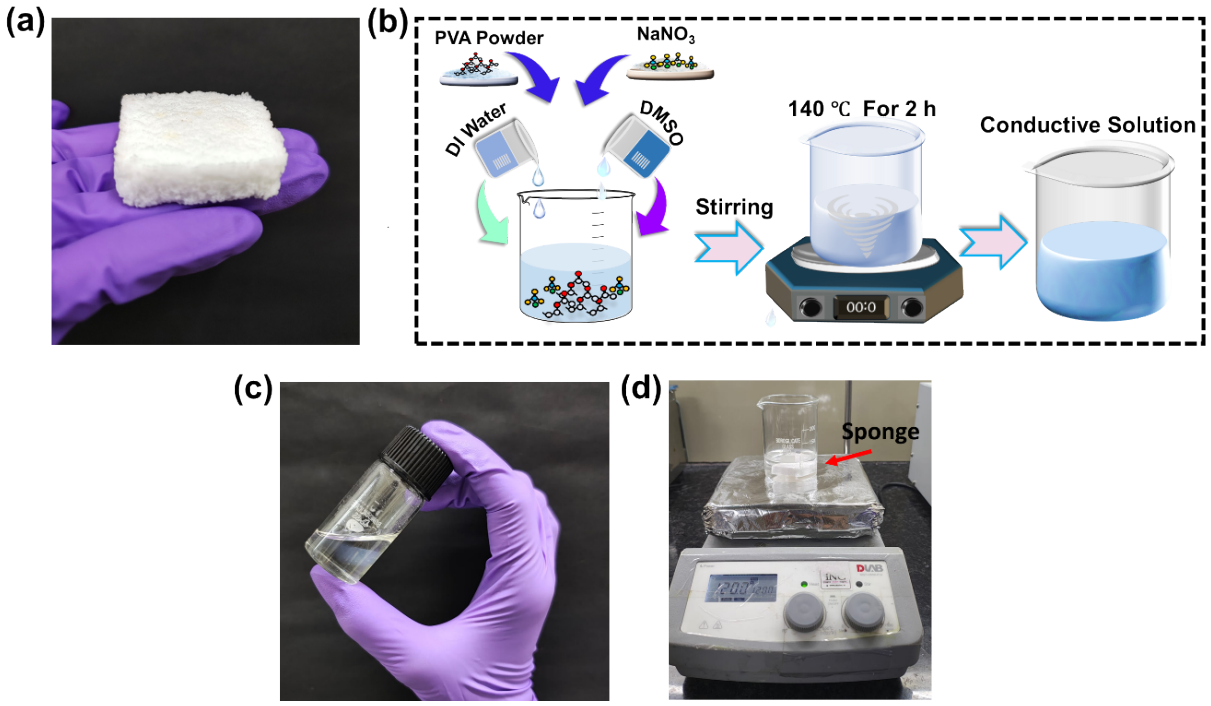

Figure S1. Pictures depicting (a) sponge matrix, (b) synthesis of conductive solution of PVA/$NaNO_3$ solution, (c) digital image of conductive gel solution, and (d) sponge immersed in the conductive solution.

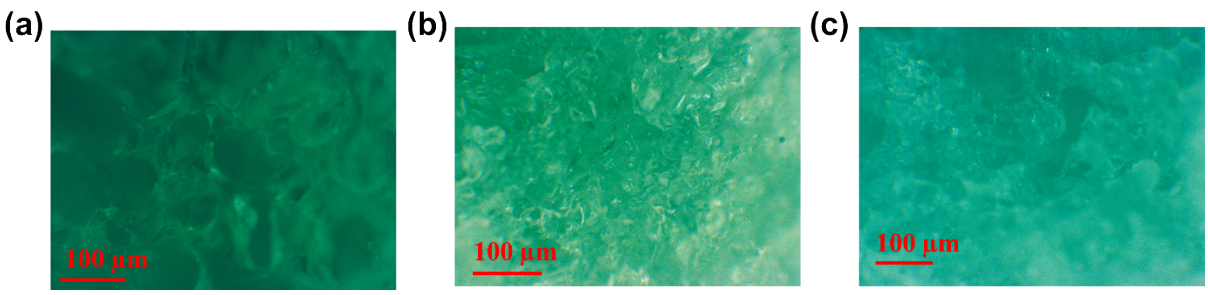

Figure S2. Microscopic images of (a) unsoaked, (b) soaked, and (c) frozend sponge.

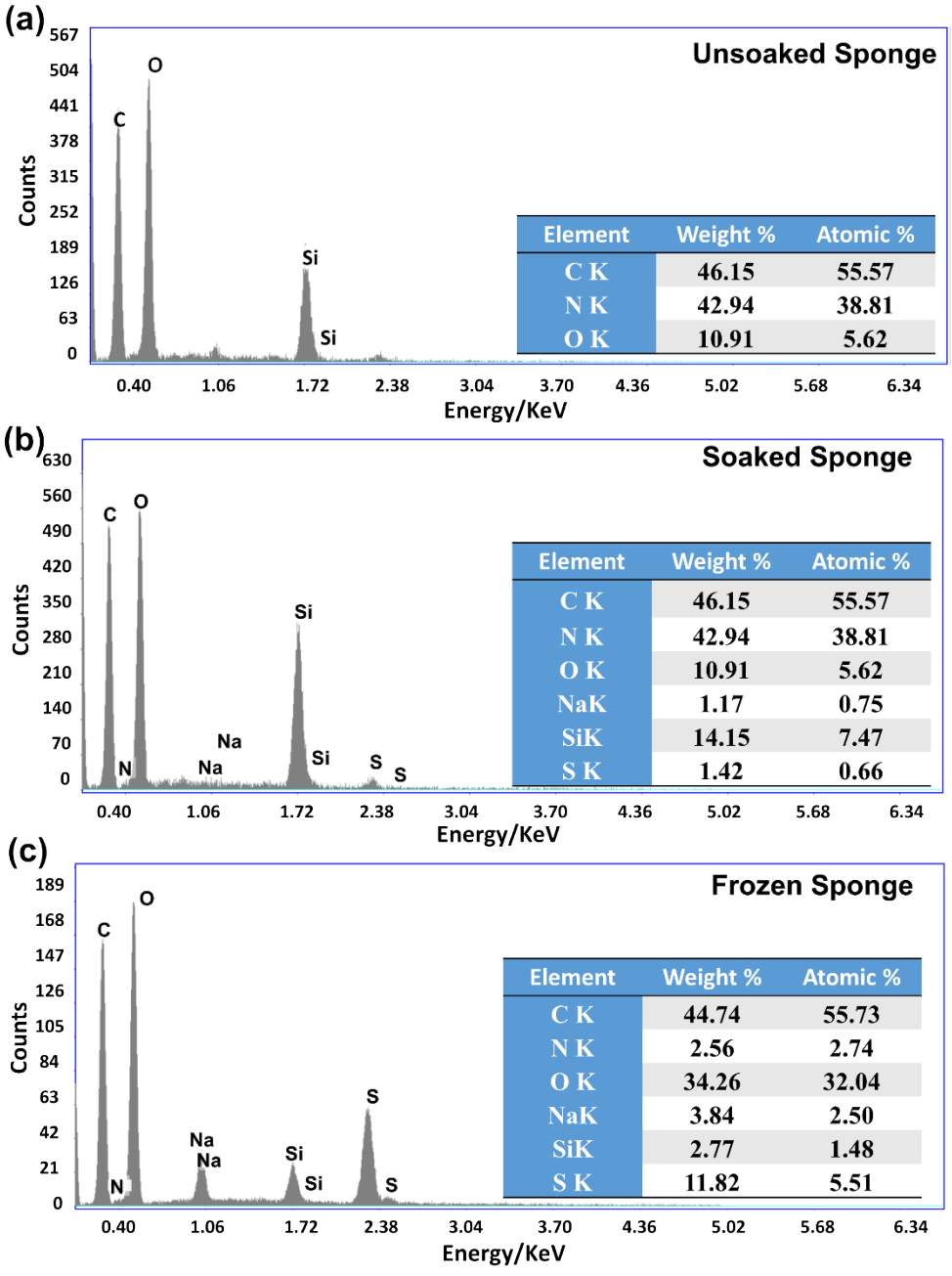

Figure S3. Graphs showing the elemental composition of (a) unsoaked, (b) soaked, and (c) frozen sponge.

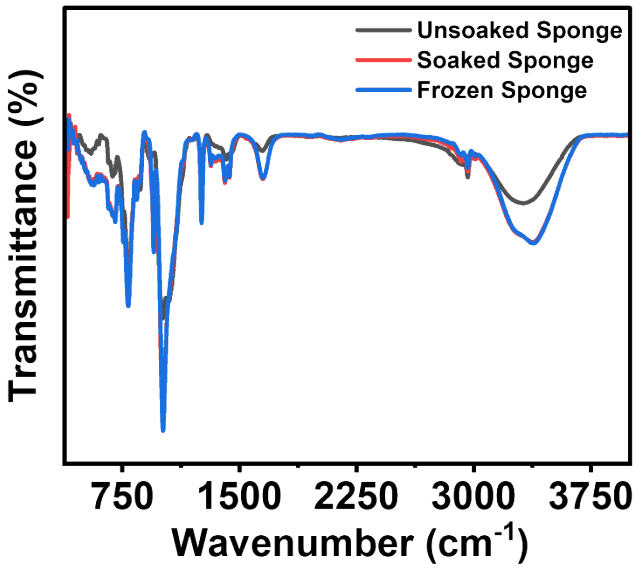

Figure S4. Comparative FTIR graph of unsoaked, soaked, and frozen sponge.

Table S1. A summarized table comparing the conductivity and error ranges of unsoaked, soaked, and frozen sponge.

Sponges	Conductivity (mS/m)
Unsoaked	0.18542 ± 0.50799
Soaked	649.28 ± 69.52987
Frozen	276.43 ± 68.61721

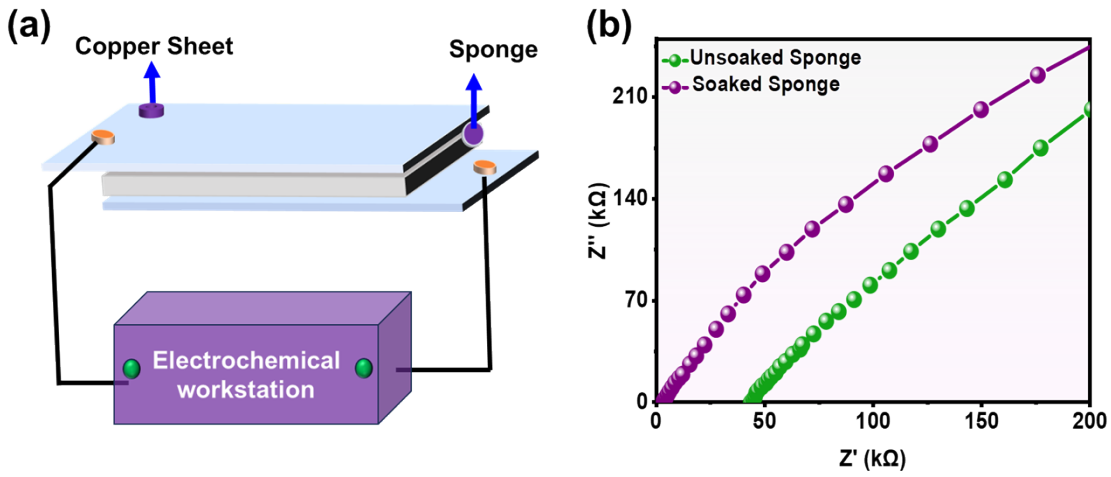

Figure S5 (a) Schematic representation of the conductivity measurement setup, where sponge samples were positioned between copper tape electrodes and interfaced with the electrochemical workstation. (b) Nyquist plots illustrating the impedance response of unsoaked and soaked sponges.

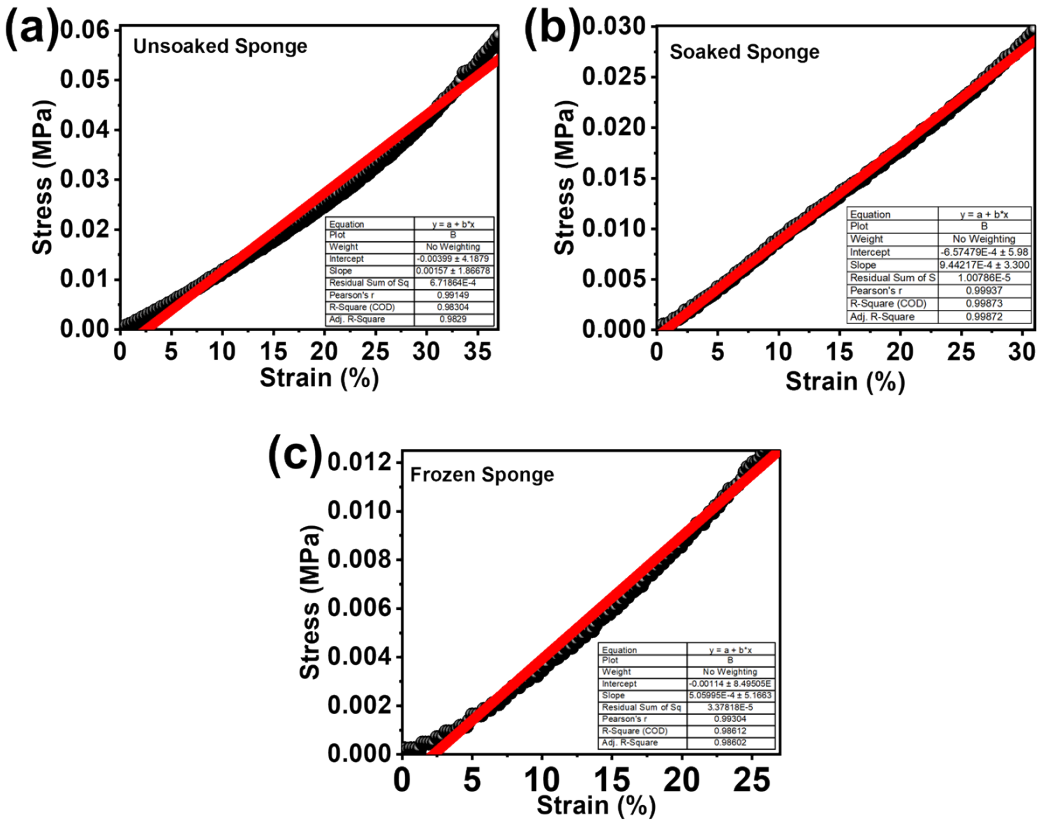

Figure S6. Plots reflecting Young's modulus from the slope of stress-strain curves for (a) unsoaked, (b) soaked, and (c) frozen sponge.

Table S2. The comparative study of compressive strength in terms of Young's modulus for all prepared sponges.

Sponges	Young's Modulus (MPa)
Unsoaked	0.18542 ± 0.50799
Soaked	649.28 ± 69.52987
Frozen	276.43 ± 68.61721

Table S3. A summarized table comparing the compressive strength of previously reported sponges

Sr. No.	Sponge	Compressive Strength (MPa)	Reference
1.	rGO/PEI/PDMS	0.11	[1]
2.	CNT-PDMS	0.099	[2]
3.	MXene/PPy@PDMS	0.061	[3]
4.	PDMS/GO	0.042	[4]
5.	PDMS/oND	0.065	[5]
6.	CS-TENG	0.10	This Work

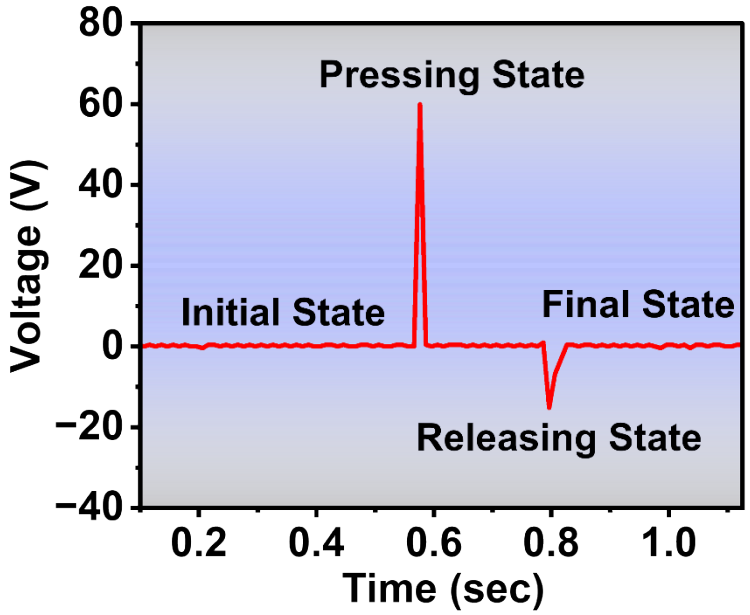

Figure S7. Mechanistic response of CS-TENG during a single-cycle pulse.

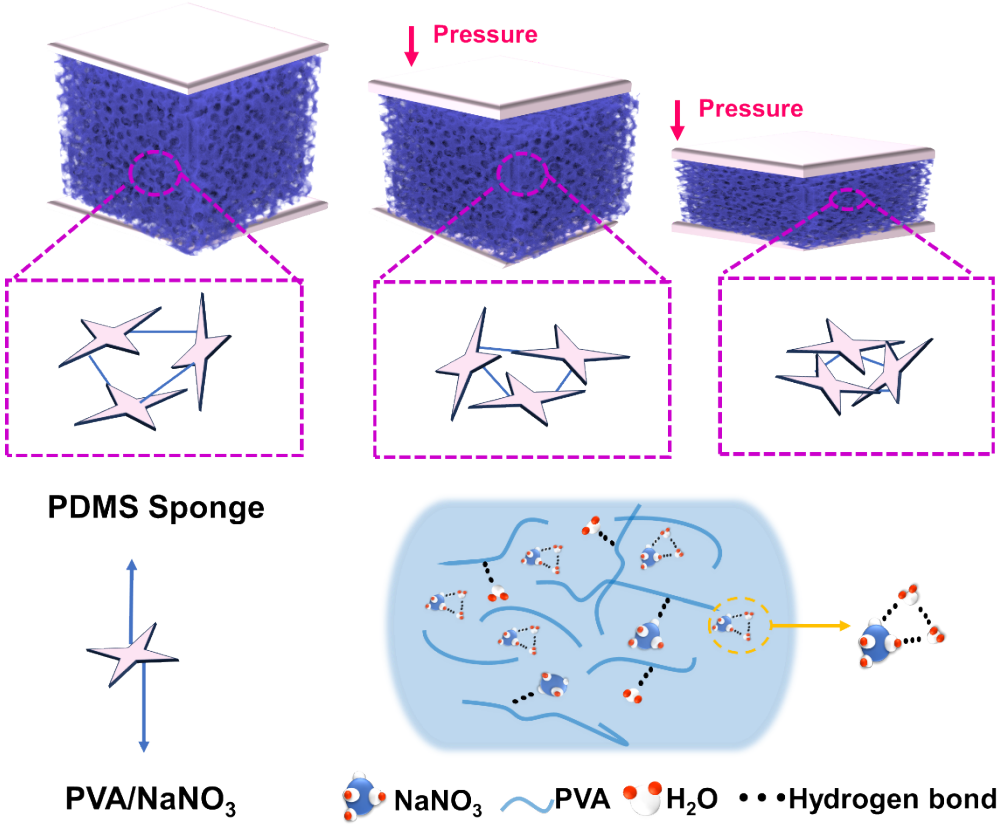

Figure S8. Pressure-sensing mechanism of the fabricated CS-TENG, illustrating the changes in contact area of the sponge framework under compressive deformation.

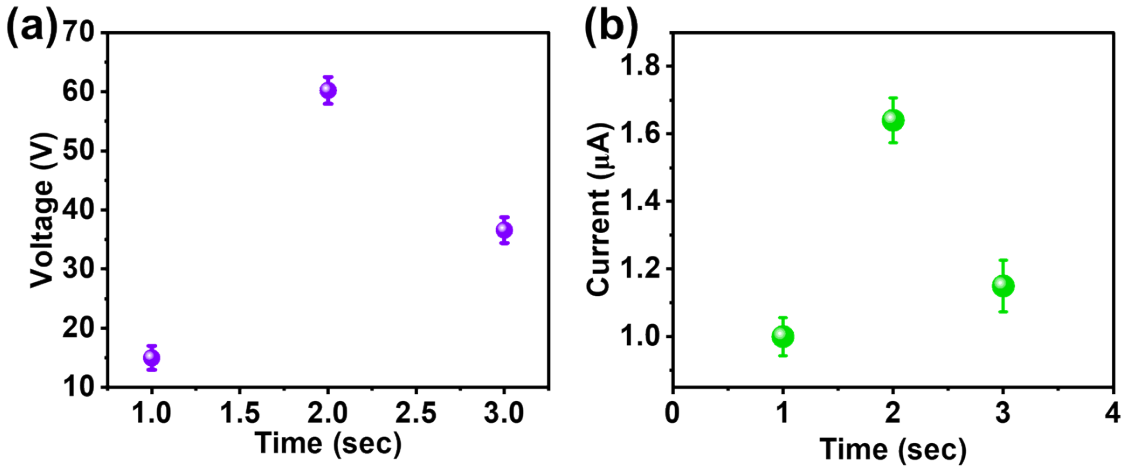

Figure S9. Plots depicting (a) output voltage performance and (b) output current of the TENG device.

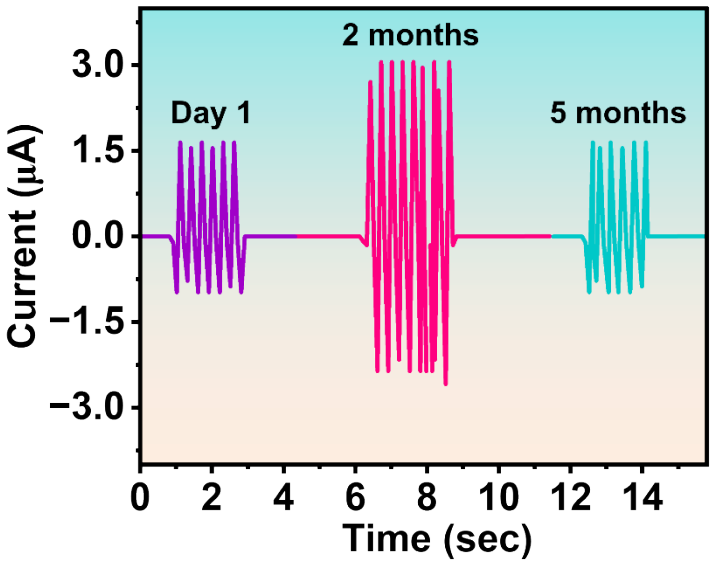

Figure S10. Graph depicting the output current performance of CS-TENG after 5 months.

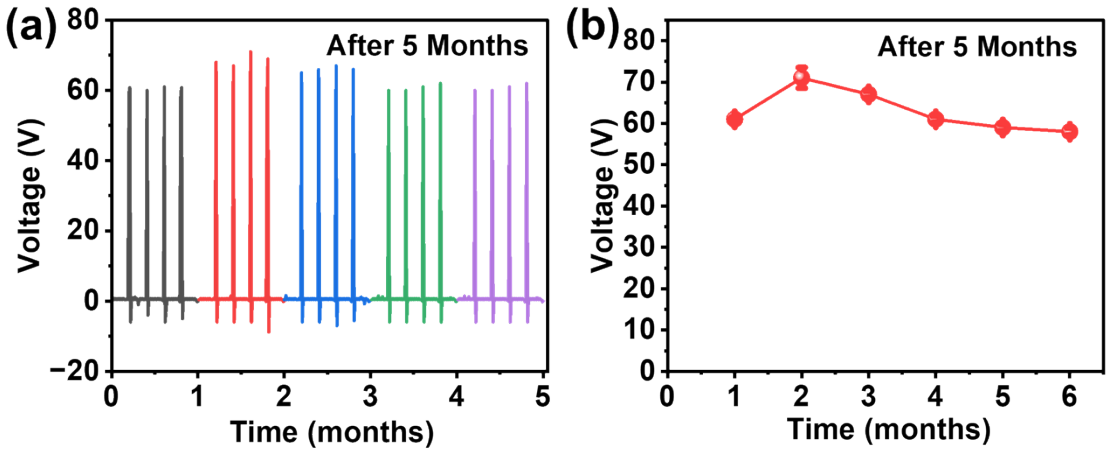

Figure S11. Plots depicting the (a,b) output voltage performance of CS-TENG after 5 months.

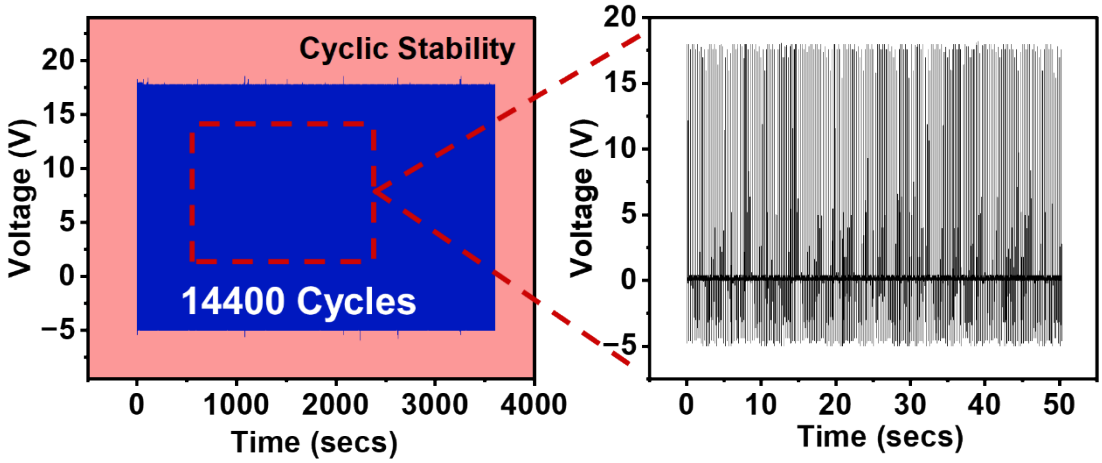

Figure S12. Cyclic stability performance of the CS-TENG over 14,400 cycles at a frequency of 4 Hz.

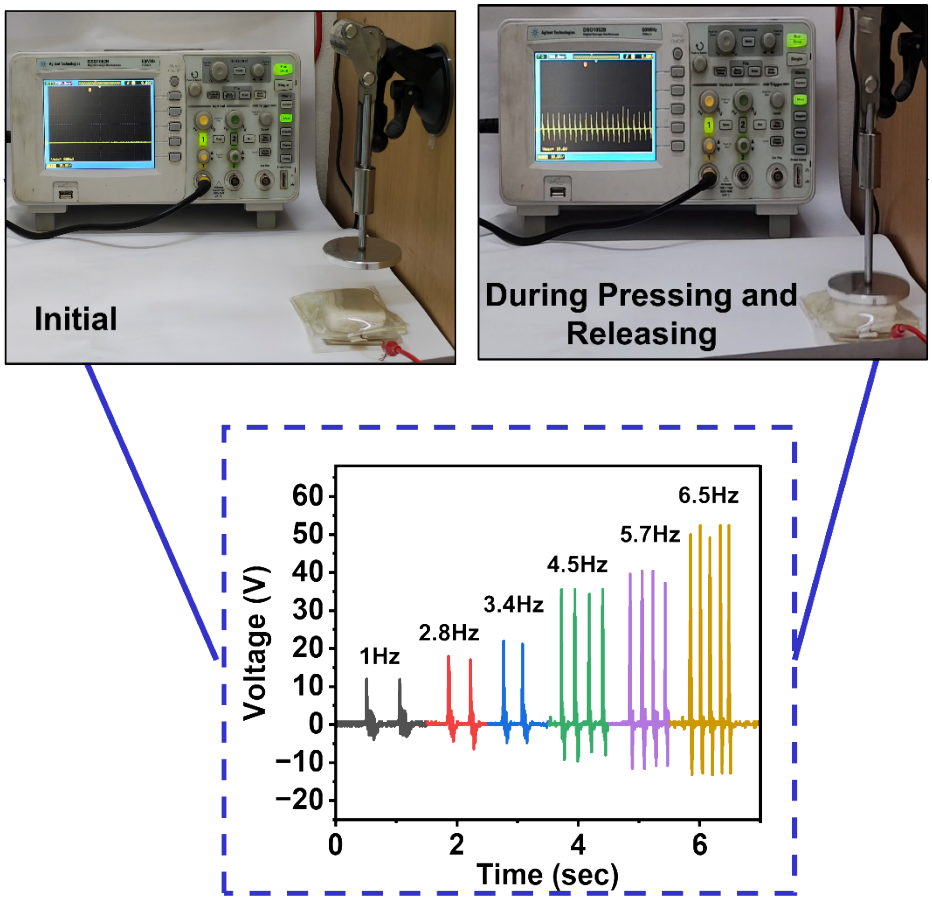

Figure S13. Plot depicting the output voltage performance under different frequencies, along with the pneumatic system showing pressing and releasing.

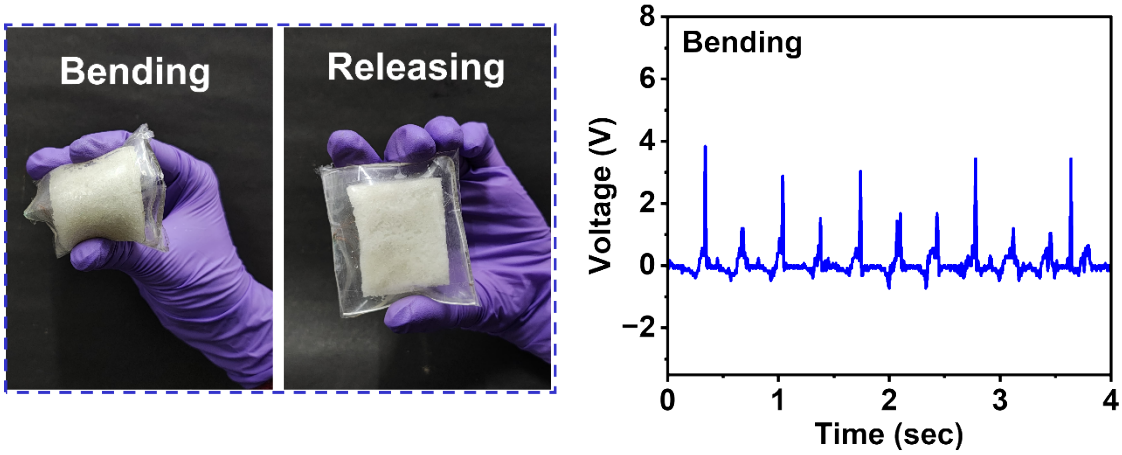

Figure S14. Bending and releasing performance of the CS-TENG in terms of output voltage.

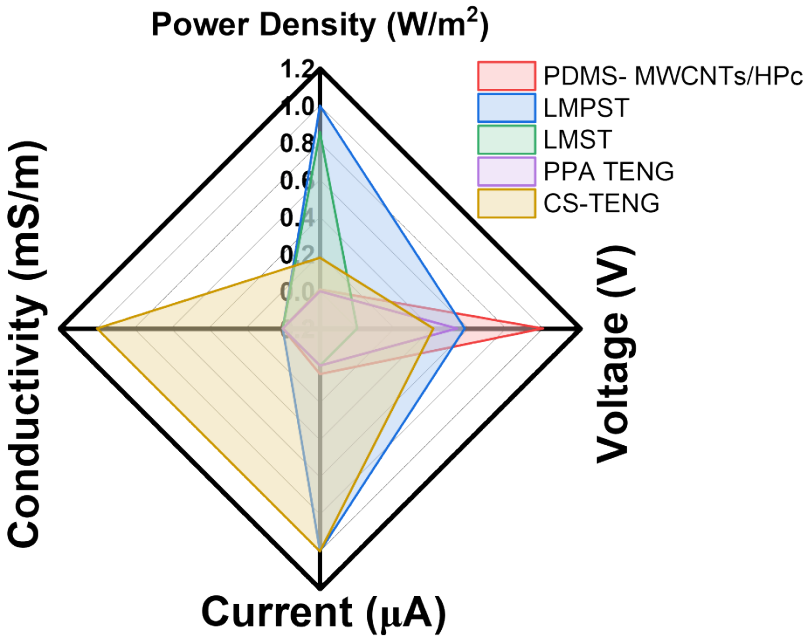

Figure S15. Radar chart illustrating a comparative analysis of output power density, conductivity, current, and voltage among previously reported sponge-based TENGs and CS-TENG.

Table S4. A summarized table comparing the output power density, conductivity, and voltage of previously reported sponge-based TENGs.

Sr. No.	Sponge-based TENGs	Power Density (W/m^2)	Voltage (V)	Current (μA)	Conductivity (mS/m)	Reference
1.	PDMS-MWCNTs/HPC	0.098	149.09	0.262	-	[6]
2.	LMPST	2.89	82	1.66	-	[7]
3.	LMST	2.48	24	0.188	-	[8]
4.	PPA TENG	0.0704	80	-	-	[9]
5.	FS-TENG	0.09895	48.19	1.243	-	[10]

6.	CS-TENG	0.588	61	1.6	649.28	This Work

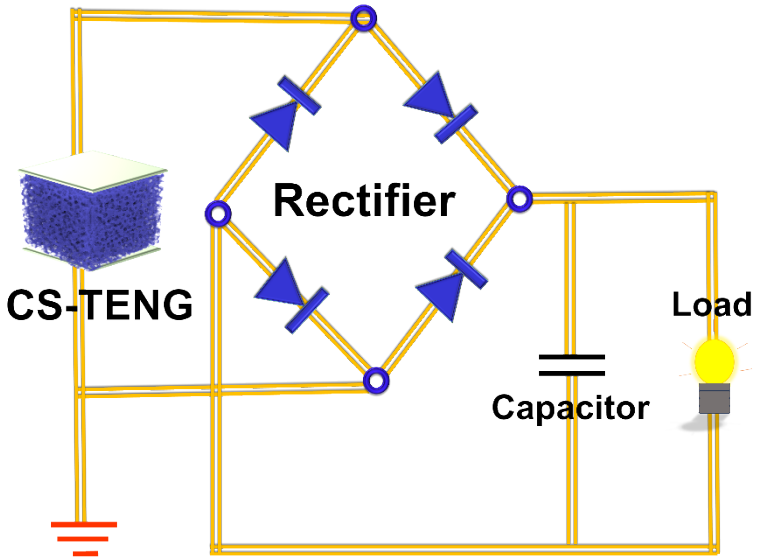

Figure S16. Schematic of the CS-TENG circuit for LED illumination and capacitor charging

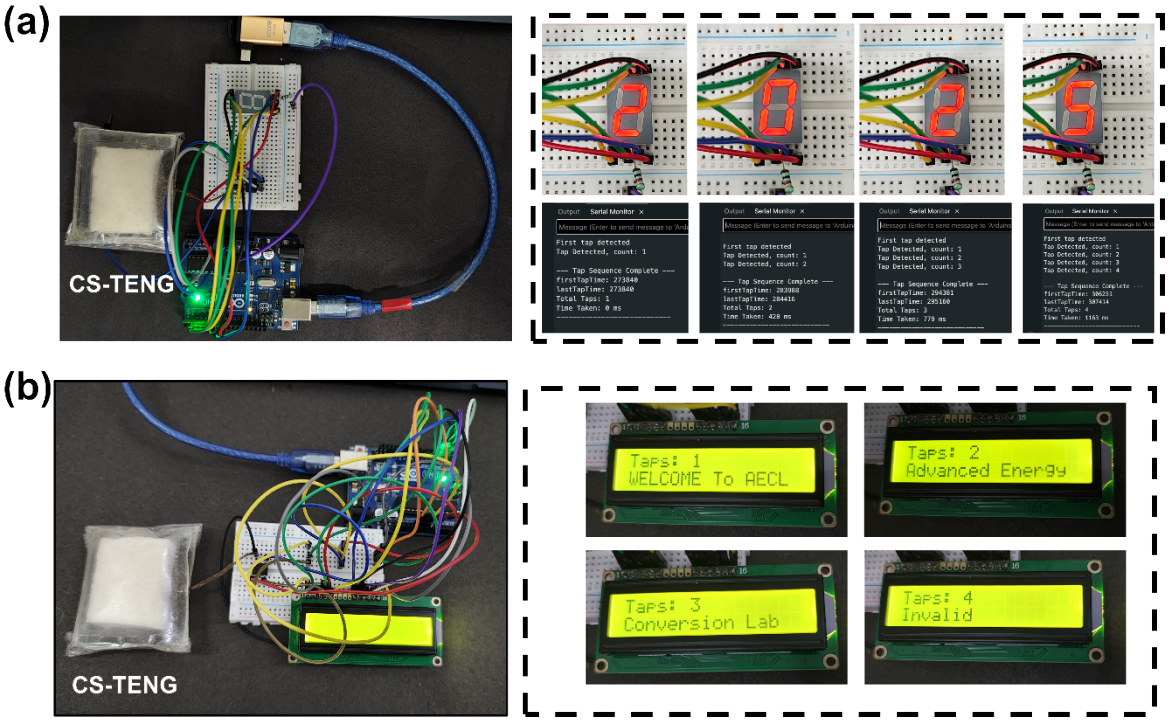

Figure S17. Demonstration of wired integration of CS- TENG with (a) 7-segment LED display and (b) 16×2 LCD.

References

[1] H. Tong, H. Chen, Y. Zhao, M. Liu, Y. Cheng, J. Lu, Y. Tao, J. Du, H. Wang, Robust PDMS-based porous sponge with enhanced recyclability for selective separation of oil-water mixture, Colloids and Surfaces A: Physicochemical and Engineering Aspects 648 (2022) 129228.
[2] Y. Song, H. Chen, Z. Su, X. Chen, L. Miao, J. Zhang, X. Cheng, H. Zhang, Highly compressible integrated supercapacitor–piezoresistance-sensor system with CNT–PDMS sponge for health monitoring, small 13(39) (2017) 1702091.
[3] H. Xia, L. Wang, H. Zhang, Z. Wang, L. Zhu, H. Cai, Y. Ma, Z. Yang, D. Zhang, MXene/PPy@ PDMS sponge-based flexible pressure sensor for human posture recognition with the assistance of a convolutional neural network in deep learning, Microsystems & Nanoengineering 9(1) (2023) 155.
[4] J. Zhao, H. Chen, H. Ye, B. Zhang, L. Xu, Poly (dimethylsiloxane)/graphene oxide composite sponge: a robust and reusable adsorbent for efficient oil/water separation, Soft Matter 15(45) (2019) 9224-9232.
[5] X. Zhao, T. Wang, Y. Li, L. Huang, S. Handschuh-Wang, Polydimethylsiloxane/nanodiamond composite sponge for enhanced mechanical or wettability performance, Polymers 11(6) (2019) 948.
[6] L. Luo, B. Zhang, Y. Lei, D. Chai, D. Zhang, K. Xu, N. Chen, S. Hu, H.-L. Peng, H. Wang, Interface-engineered porous PDMS-MWCNTs composites through HPC-mediated "sponge pump absorption" strategy for high-performance triboelectric nanogenerators, Materials Today Communications 44 (2025) 112192.
[7] Y. Wang, C. Zhao, L. Chen, Q. Wu, Z. Zhao, J.-J. Lv, S. Wang, S. Pan, M. Xu, Y. Chen, Flexible, multifunctional, ultra-light and high-efficiency liquid metal/polydimethylsiloxane sponge-based triboelectric nanogenerator for wearable power source and self-powered sensor, Nano Energy 127 (2024) 109808.
[8] J. Park, I. Kim, J. Yun, D. Kim, Liquid-metal embedded sponge-typed triboelectric nanogenerator for omnidirectionally detectable self-powered motion sensor, Nano Energy 89 (2021) 106442.
[9] Y. Guan, W. Yang, L. Yang, H. Wang, Z. Xi, Y. Kang, Z. Zhao, C. Zhu, L.F. Petrik, M. Shen, A self-powered Triboelectric Nanogenerator for Energy Collection Based on polydimethylsiloxane/Dopamine/Ag nanowires Porous Materials formed by manganese carbonate, Colloids and Surfaces A: Physicochemical and Engineering Aspects (2025) 137174.
[10] H. Cho, S. Jo, I. Kim, D. Kim, Film-sponge-coupled triboelectric nanogenerator with enhanced contact area based on direct ultraviolet laser ablation, ACS applied materials & interfaces 13(40) (2021) 48281-48291.